12-2021

Soil Structure and Soil Moisture Dynamics Inferred from Time-Lapse Electrical Resistivity Tomography

Travis Nielson
Boise State University

John Bradford
Boise State University

Jen Pierce
Boise State University

Mark Seyfried
United States Department of Agriculture – Agricultural Research Service

Publication Information

Nielson, Travis; Bradford, John; Pierce, Jen; and Seyfried, Mark. (2021). "Soil Structure and Soil Moisture Dynamics Inferred from Time-Lapse Electrical Resistivity Tomography". *Catena, 207*, 105553.
https://doi.org/10.1016/j.catena.2021.105553

Catena 207 (2021) 105553

Contents lists available at ScienceDirect

Catena

journal homepage: www.elsevier.com/locate/catena

Soil structure and soil moisture dynamics inferred from time-lapse electrical resistivity tomography

Travis Nielson [a,c,*], John Bradford [b,c], Jen Pierce [c], Mark Seyfried [d]

[a] Olson Engineering, United States
[b] Colorado School of Mines, United States
[c] Boise State University, United States
[d] United States Department of Agriculture – Agricultural Research Service, United States

ARTICLE INFO

Keywords:
Soil infiltration
Electrical resistivity tomography
Seismic refraction
Preferential flow path
Critical zone

ABSTRACT

The semi-arid sagebrush steppe in the western United States faces pressures from the agriculture industry, recreation use, invasive grasses, and a changing climate. A key to facilitating the healthy management of this ecosystem is understanding the distribution and behavior of soil moisture in the vadose zone in both natural and agricultural settings. Within unsaturated environments, soil moisture is spatially and temporally heterogeneous, and changes in porosity and permeability within arid soils complicate characterization of soil hydrologic properties. Importantly, accumulations of 'caliche' or pedogenic calcium carbonate in arid soils can greatly limit permeability; however, observing the role that caliche plays in the hydrologic process is difficult because the installation of *in situ* instruments disturbs the soils and only provides information at a single point. To investigate vadose zone processes on a broad temporal and spatial scale, we installed a 7x8m^2 electrical resistivity tomography (ERT) array at the Reynolds Creek Critical Zone Observatory in southwestern Idaho. Existing soil moisture observations show that infiltration is limited to depths less than 60 cm at this site, as compared to at least 90 cm at other sites in the watershed. To capture the seasonal wetting and drying of the soils, as well as the soils' response to rainfall events, we monitored the site bi-weekly during the spring, summer, and fall of 2015 and 2016. A time-lapse ERT array was placed adjacent to coaxial impedance dielectric reflectometry (CIDR) probes so that the time-lapse ERT data could be referenced to precise measurements of volumetric water content. In addition to the measurements provided by the ERT array and CIDR probes, soil texture analysis and soil profile descriptions from a near-by soil pit show typical arid soil morphology, with accumulations of clays and calcium carbonate in the B horizon. The resulting ERT inversions show the following soil structure: (1) a high-resistivity top layer corresponding with minor amounts of pedogenic calcium carbonate; (2) a low-resistivity intermediate layer at depths corresponding with substantial accumulations (stage IV) of carbonate; and (3) a high-resistivity deep saprolite. The resistivity of the top layer varies seasonally with changes in precipitation, while the intermediate carbonate soil layer does not. This agrees well with the changes in soil moisture with depth measured by the CIDR probes and suggests that the top of the carbonate soil layer limits infiltration. However vertical structure and cracks within the carbonate soil layer create vertical preferential flow paths; resistivity within these flow paths responds to large precipitation events and seasonal changes in soil moisture. This implies that the preferential flow paths are a conduit for soil moisture flow that is not captured by the CIDR probes. From the combined interpretation of the ERT and CIDR we conclude that soil structure and the presence of calcic soil horizons inhibits soil moisture infiltration during both the summer dry months and the winter wet flux period; however, preferential flow paths provide an important vertical connection between the deep and shallow portions of the critical zone.

* Corresponding author.
E-mail address: travisnielson@u.boisestate.edu (T. Nielson).

https://doi.org/10.1016/j.catena.2021.105553
Received 27 October 2019; Received in revised form 27 May 2021; Accepted 18 June 2021
Available online 10 July 2021

1. Introduction

Semi-arid sagebrush steppe ecosystems provide valuable rangeland resources throughout large areas of the western USA. Measuring the distribution and behavior of soil moisture in the vadose zone is essential for understanding a variety of hydrologic processes in natural and agricultural settings. Within semi-arid and arid environments the hydrologic connectivity within the vadose zone has an effect on stream flow dynamics, groundwater recharge, and ecology (Freer et al., 2002; Hinckley et al., 2014; McNamara et al., 2005). However, within unsaturated environments, soil moisture is both spatially and temporally heterogeneous, making its robust characterization difficult. For example, studies in a semi-arid, xeric experimental watershed in southwestern Idaho, USA, show seasonal states of soil moisture connectivity: a dry period characterized by low and stable soil moisture; a transitional wetting period in which the field capacity is met for the deeper soils and the soil water progresses downward; a wet, low-flux period in which accumulated snow keeps soil moistures stable at around field capacity; a wet, high-flux period in which the snow begins to melt and the soil moisture responds to precipitation; and a transitional late-spring drying period after the snow melts in which soil moistures decrease from evapotranspiration (McNamara et al., 2005). However, at the plot scale the heterogeneity of soils and the potential presence of preferential flow paths complicate the characteristics of these seasonal states.

Conventional *in situ* sensors can provide accurate measurements of soil moisture at a single point and remote sensing methods provide spatially continuous measurement on the scale of kilometers. In contrast, geophysical methods can provide precise soil moisture estimates at the 1 m to 100 m scale (Robinson et al., 2008). Electrical resistivity tomography (ERT) is one of the most common geophysical methods for characterizing soil moisture, making it sensitive to short and long-term soil moisture changed. In addition, the ERT electrode arrays can be installed permanently thereby reducing the impact of each measurement, which is ideal for non-invasive time-lapse applications.

The application of electrical methods to characterize changing soil moisture dates to before the use of tomographic inversions. One of the earliest applications of DC electrical methods to soil science was by Kean et al., (1987), who used vertical electrical sounding to characterize soil moisture migration before and after rainfall events. Daily et al. (1992) applied tomographic inversion methods to create a two-dimensional perspective of unsaturated flow in the vadose zone. By applying tomographic inversions (Daily et al., 1992) opened the door for more broad scale characterization of soil moisture heterogeneity. Now with the relatively low cost of electrical resistivity controllers and sophisticated readily available tomographic inversion software, ERT is widely applied to vadose zone water infiltration. Modern ERT allows for broad scale measurements that capture the spatial heterogeneity that would not be practical to characterize with point scale measurements, such as soil moisture probes, and more detailed measurements than are possible with remote sensing methods. Further, the use of surface arrays allows for continuous observations without interfering with the natural flow patterns.

Previous studies have demonstrated the application of ERT for imaging seasonal monitoring of soil moisture changes (Amidu and Dunbar, 2007; Brillante et al., 2014; Brunet et al., 2010; Calamita et al., 2012; Fan et al., 2015; French and Binley, 2004; Miller et al., 2008; Niemeyer et al., 2017; Nijland et al., 2010; Robinson et al., 2012; Schwartz et al., 2008; Yamakawa et al., 2012) and the imaging preferential flow path structure (Leslie and Heinse, 2013). Currently, the application of ERT towards the vadose zone can be loosely broken into three categories, controlled infiltration experiments for technical development (Kean et al., 1987; Daily et al., 1992; Al Hagrey et al., 1999; Al Hagrey and Michaelsen, 1999; Dietrich et al., 2003; Singha and Gorelick, 2005; Cassiani et al., 2006; Deiana et al., 2007; Monego et al., 2010; Travelletti et al., 2012; Zumr et al., 2012) and the observation of infiltration from crop irrigation (Michot et al., 2003; Srayeddin and Doussan, 2009) and meteoric precipitation (Amidu and Dunbar, 2007; Brillante et al., 2014; Brunet et al., 2010; Calamita et al., 2012; Fan et al., 2015; French and Binley, 2004; Miller et al., 2008; Niemeyer et al., 2017; Nijland et al., 2010; Robinson et al., 2012; Schwartz et al., 2008; Yamakawa et al., 2012). The majority of these ERT experiments have been conducted in Europe, with only a handful in the US, and only one ERT experiment (Miller et al., (2008) has observed the seasonal variation in soil moisture in the western sagebrush steppe. However, Miller et al. (2008) focused on the deeper vadose zone seasonal moisture dynamics, leaving the imaging of the shallow seasonal changes and response to natural precipitation events within the sagebrush steppe unexplored with ERT.

Preferential flow paths provide a hydrologic pathway, other than matrix flow that contributes to subsurface flow (Tromp-van Meerveld and McDonnell, 2006a, 2006b). Understanding their distribution and dimensions has large implications for hillslope hydrologic modeling (Sidle et al., 2001). However, the majority of previous work on preferential flow paths has relied on excavation and dye tracer observations, which disrupt the existing soil textures making long term observations in a natural environment difficult (Leslie and Heinse, 2013). High-resolution ground penetrating radar and ERT have been used to image preferential flow paths (Leslie and Heinse, 2013) and fractures (Hansen and Lane, 1995; Robinson et al., 2013). Uhlemann et al. (2017) successfully time-lapse ERT to characterize preferential flow paths response to seasonal and precipitation changes of a landslide, but time-lapse ERT has previously not been used to characterize preferential flow in a sagebrush steppe.

This project examines the spatial temporal variation in hydrologic connectivity within the vadose zone by using ERT to image the changes in soil moisture in response to seasonal changes and precipitation events. We installed a permanent 3D ERT array (7 m by 8 m) at a site within the Reynolds Creek Critical Zone Observatory (RCCZO) in southwestern Idaho, USA, and used it to conduct ERT surveys about every two weeks from May of 2015 to June of 2016. To constrain the broader soil and critical zone structure, we also acquired a pair of crossing 2D seismic refraction tomography (SRT) and 2D ERT surveys overtop the 3D ERT array. While other studies have applied electrical methods to understanding soil moisture distribution at the RCCZO (Niemeyer et al., 2017; Robinson et al., 2012), this is the first high temporal density ERT surveys at the RCCZO. Additionally, this study is the first 3D ERT study to monitor seasonal and precipitation driven changes in shallow soil moisture within the western sagebrush steppe.

2. Site-description

The RCCZO is a 240 km^2 experimental watershed in southwest Idaho. Geologically the RCCZO is primarily underlain by Cretaceous granitic material from the Idaho Batholith. Miocene volcanism deposited basalts and andesites over the batholith, followed by additional episodes of late Miocene/early Pliocene volcanism which deposited basalts, latites, and welded tuffs over large portions of the southern watershed (McIntyre, 1972). During Quaternary to Pliocene times, four alluvial terraces parallel Reynolds Creek in its northern reaches, as well as some exposures of lake deposits and delta sequences (Stanbery, 2016). On the more stable alluvial and arkosic surfaces, soils are generally more well-developed (Stanbery, 2016).

Our study examined critical zone characteristics at a flat-lying, low elevation site within the watershed (1406 m) dominated by sagebrush (*Artemisia tridentada ssp*) and grasses (Fig. 1). The bedrock at this Low Elevation Sagebrush (LES) site is mapped as basalt (McIntyre, 1972); widespread deposition of loess provides the primary parent material for soils at this site (Stanbery, 2016; Stanbery et al., 2017). The site is near a northerly-flowing ephemeral stream within a topographic basin. Climatically, the RCCZO is a xeric site dominated by winter rain and snow. At the LES site, rain is the dominant form of precipitation, with occasional snow in the winter.

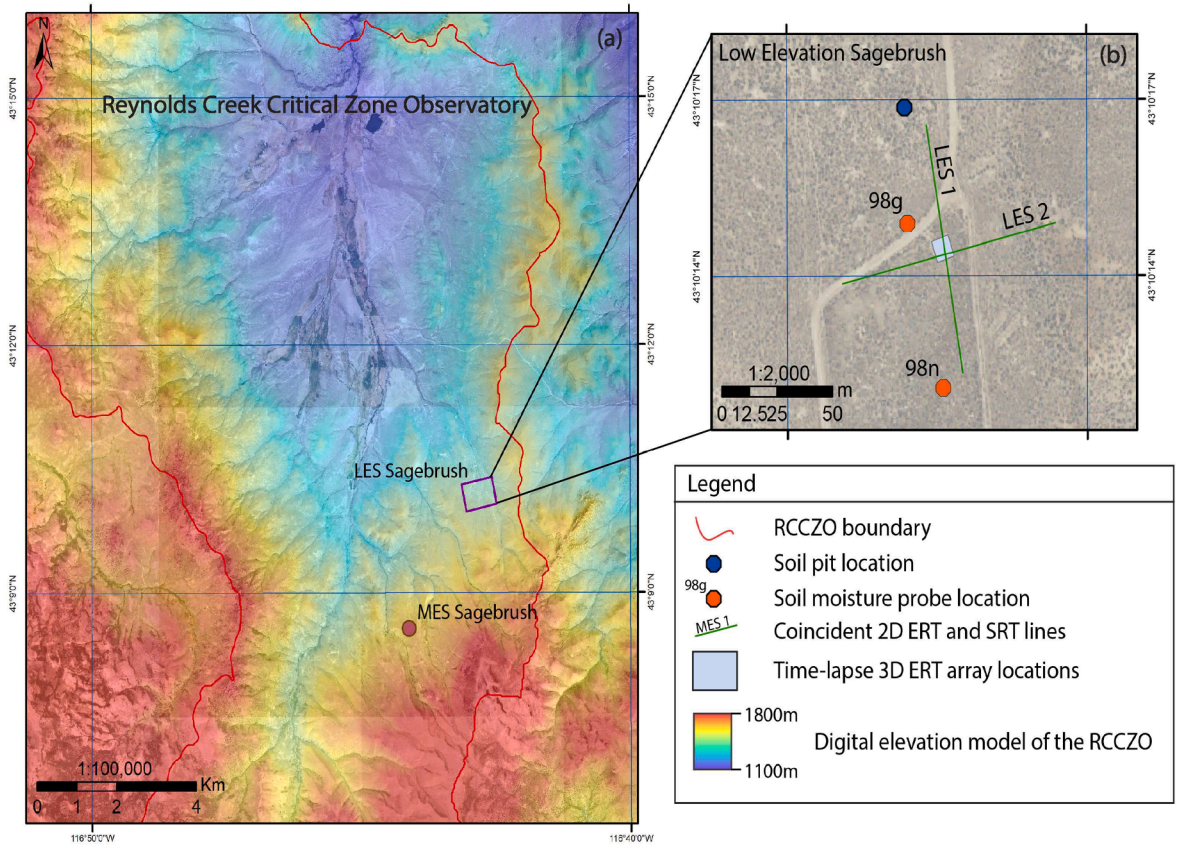

Fig. 1. (a) is a digital elevation model overlaying satellite images of the southern portion of the Reynolds Creek Critical Zone Observatory, with the Reynolds Creek watershed boundary shown as a red line. The approximate extent of the LES site is shown as purple squares in (a) and the location of the MES site is shown as a purple circle. (b) is a satellite image map of the LES sites, with the 2D SRT and 2D ERT surveys lines, the extent of the 3D ERT surveys, and soil moisture probe proles locations 98n and 98 g shown. (For interpretation of the references to color in this figure legend, the reader is referred to the web version of this article.)

Two profiles of Stevens hydraprobes (CIDR probes) are installed at LES. One within a cattle exclosure (given the suffix *n* for non-grazed), and one outside the exclosure (given the suffix *g* for grazed, Fig. 1). The CIDR probes log volumetric water content every 15 min at depths 5 cm, 15 cm, 30 cm, 60 cm and 90 cm. The volumetric water content within the exclosure and the precipitation amount for the site are shown in Fig. 2.

3. Methods

To image the changes in electrical resistivity caused by the changes in soil water content we installed a permanent ERT array. The permanent 3D ERT array consists of 72 electrodes arranged in a uniform rectangular 8 × 9 grid; the electrodes are buried ~6 cm deep and spaced 1 m from each other, resulting in a 7 × 8 m array. Each electrode is wired to a central connection box placed in the center of the array. The surveys were conducted using an Iris Syscal Pro Switch resistivity meter. A total of 303 single axis dipole–dipole measurements in both the x and y direction were collected with electrode pair separations varying from 1 m to 6 m. The electrodes are composed of stainless-steel wool connected to the wire via stainless steel nuts and bolt. To capture the seasonal changes in resistivity, the surveys were conducted once every two weeks during the spring of 2015 and the fall of 2015, and weekly during the spring of 2016.

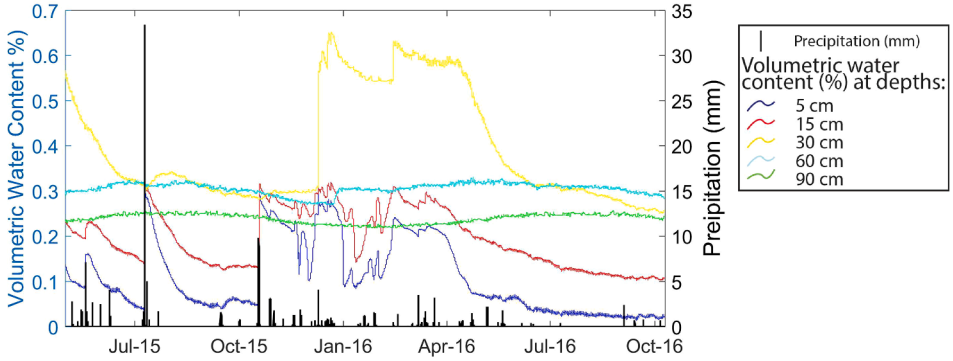

Fig. 2. The colored lines are the volumetric water content as measured at the LES site by CIDR probes at location 98n, shown in Fig. 1. The volumetric water content from location 98n is shown because it is within the cattle exclosure that contains the ERT array. The precipitation is shown as black vertical lines. Despite receiving a similar amount of precipitation as the MES site (Fig. 3) the volumetric water content at 60 cm and 90 cm remains largely constant.

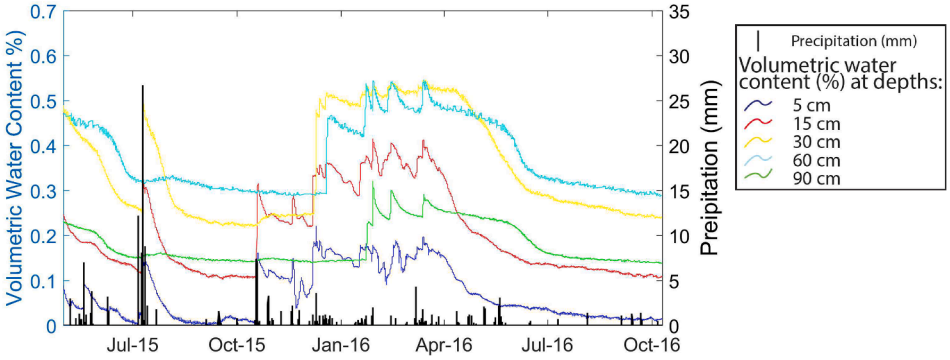

Fig. 3. The colored lines are the volumetric water content as measured by at the MES site by CIDR probes. The precipitation is shown as black vertical lines. Unlike the LES site the CIDR probes at 60 cm and 90 cm measure changes in volumetric water content. As in the LES site, these CIDR probes are also within a cattle exclosure.

The apparent resistivities were inverted using an iteratively reweighted least squares inversion with the software package E4D (Johnson et al., 2010). The inversions were performed using a time-lapse approach with the result of a static inversion is used as a reference model. For both the static and time-lapse inversions the weighting matrix W is calculated using:

$$W = 1/2\left(1 - erf\left((X + mn)/\sqrt{2sd^2}\right)\right) \quad (1)$$

where *erf* refers to the Gauss error function, *mn* is the center of the error function, and *sd* the standard deviation. X is referred to as the structural metric, for the static inversion is defined by:

$$X = |m_t - m_n| \quad (2)$$

where m_t and m_n are the log of the conductivities of the target element and its spatial neighbor. The effective width equation (1) is $mn + 2sd$; ergo if X is greater than $mn + 2sd$ full weighting is applied and if X is less than mn-$2sd$ no weighting is applied. To allow for some heterogeneity to develop in the model while still suppressing artifacts the *mn* and *sd* used in Eq. (1) were 4 and 1, respectively. Static inversions were performed on the surveys gathered from February 23rd, 2016 and June 23rd, 2016. This insured that the resistivity structures are persistent. The static inversions were iterated until the χ^2 of the modeled and measured apparent resistivity are less than 1.5 after erroneous data is culled.

As with the static inversion, Eq. (1) was used to determine weighting matrix W. However, the structural metric was calculated using the current grid and a reference model:

$$X = \left|\left(m_t - v_{ref}\right) - \left(m_n - v_{refn}\right)\right| \quad (3)$$

where m_t and m_n are the log of the conductivities of the target element and its spatial neighbor; and v_{ref} and v_{refn} are the log of conductivity of the target element and its spatial neighbor in a reference model. The *mn* and *sd* used in Eq. (1) for the time-lapse inversion were 0 and 2, respectively. This weighting schema acts to smooth the difference between the reference and the target grid, and thus forcing a consistent resistivity structure. As can be deduced, the quality of the time-lapse inversion result is dependent on the quality of the reference model used to build the weighting matrix W. We assume that the changes in resistivity will be a function of changes in soil moisture. Thus, we use a static inversion result taken when the soil moisture is at its minimum for the reference model. This means that the difference in resistivity between the target and reference model will all be negatives and can be attributed to changes in soil moisture. The reference model from the lower moisture state was used, as opposed to a reference model from a high moisture state, because the sensitivity at depth is higher at periods of low moisture. The June 29th, 2016 survey was chosen to be the reference solution, as it was during a low soil moisture period and the static inversion converged to a high degree of confidence, $\chi^2 = 1.107$. The time-lapse inversions were iterated until the objective function reduced by less than 0.00001 between iterations.

The mesh used for both inversions us 12 m × 12 m × 5 m, well beyond the extent of the array and depth of investigation. The size of the mesh was chosen through trial and error to be the smallest mesh that would not produce edge effects. The area of confidence is an 8 m × 8 m × 1.5 m grid. To produce a smooth image for plotting, the inversion results are interpolated to a uniform 0.05 m grid spacing. No additional constraints were applied to either the time-lapse or static inversions

Since soil temperatures at the LES site vary from −2 °C in the winter, to 30 °C in the summer, a temperature correction was performed to normalize the resistivities to a single temperature. If the resistivities were not corrected for, then comparing the resistivity models across seasons would be skewed, as resistivity decreases with increasing temperature. The soil temperatures were corrected using the method outlined by Keller and Frishchknecht, (1966), who proposed the resistivities can be adjusted to a temperature using:

$$\rho_{25} = \rho_m\left[1 + 0.02\left(T_m - T_{ref}\right)\right] \quad (4)$$

where ρ_{25} is the corrected restively, ρ_m is the measured resistivity, $T_m$is the temperature during the measurement, and T_{25} is the reference temperature (25 °C in this study). Soil temperature is measured at depths of 5 cm, 10 cm, 20 cm, 30 cm, 40 cm, 50 cm, 60 cm, 90 cm, 120 cm, and 180 cm at the site; although outside of the map extent in Fig. 1. A piecewise cubic hermite interpolating polynomial was fitted to the measured temperatures at 5 cm spacing, and it was assumed that the ground temperature is 11.1 °C at 10 m depth year-round. Thus, a 1D T_m was generated with the same vertical spacing as the resistivity tomograms.

To understand the broader resistivity structure, a pair of 2D ERT surveys were conducted overtop and parallel to the edge of the 3D ERT arrays, see Fig. 1 for 2D and 3D survey extents. The surveys were conducted on October 6th, 2016. For the 2D ERT surveys, a 72 electrode array with 2 m electrode spacing was used and the surveys were conducted using an Iris Syscal Pro Switch. A combined total of 1646 dipole–dipole and Wenner array measurements were made. On the same day as the 2D surveys the 3D arrays were also used to perform a 3D survey. The measured apparent resistivities were inverted with a smoothness-constrained Gauss-Newton least-squares inversion (Sasaki, 1992) using the software package Res2Dinv. The inversions were completed with 10 iterations, which was enough for the RMSE between iterations to change by less than 1%. We chose to use Res2Dinv rather than E4D for the 2D inversion because it is widely used; in addition, two different inversion methods provide an additional check on our results.

In addition to the 2D ERT, we gathered 2D seismic refraction surveys (SRT) to contain the broader CZ structure. By employing both ERT and

SRT, the CZ structure can be more robustly interpreted. We conducted 2D SRT surveys on the same day and at roughly the same extent and orientation as the 2D ERT surveys (Fig. 1). The SRT surveys consisted of 96 10 Hz geophones spaced 1.5 m apart with 9 stacked shots performed every 6 m using an 8 lb sledgehammer and aluminum plate. The first arrivals were inverted with a wavepath eikonal traveltime tomography inversion (Schuster and Quintus-Bosz, 1993), using the Rayfract software package. The inversion was allowed 150 iterations. While the relationship between the weathering state and seismic velocity of granite is well established (Holbrook et al., 2014; Olona et al., 2010), this relationship is not well defined for the basaltic weathering process. However the knowledge that decreasing p-wave velocity correlates to increasing weathering (Parsekian et al., 2015) is used to inform our interpretations of the 2D resistivity structure.

To supplement the 3D ERT grids a soil pit was dug to a depth of 1.1 m at the location shown on Fig. 1. The pit was dug outside of the cattle exclosure to avoid disturbing other long-term experiments that were being conducted within the exclosure. The soil horizons were analyzed in the field for their soil texture, carbonate stage, gravel percent, grain structure, color, and consistency. Additional samples were taken to analyze the water fraction.

4. Results

The resistivity models from the static inversion soil moisture taken during the winter wet interval (February) and summer dry interval (June) show that while the soil moisture states are very different at the times these two surveys were taken (Fig. 2), the resistivity structure remains largely the same (Fig. 4). The changes in 1D resistivity with depth also correlate with the soil horizons found in the adjacent soil pit (Fig. 4).

The static 3D ERT inversions all converged to a mean residual of less than ±0.05 Ωm and a χ^2 of 1.1 or less. The time lapse inversions converged to a mean residual of less than 0.1 Ωm and a χ^2 of 4.5 or less. The higher level of convergence in the static inversion is due to the lack of temporal constraint, which allows the resistivity structure to vary and fit the measured apparent resistivities more closely. However, the time-lapse inversion is preferred for hydrologic analysis, as the temporal constraint ensures smooth temporal changes that better reflect seasonal changes in soil moisture. The static inversions (Fig. 4) show variable resistivity values; however, the soil structures are largely the same. This suggests an inherent resistivity structure to the soils. All the 2D ERT surveys were inverted to a mean residual of less than 0.5 Ω m, and the 2D seismic refraction converged to solutions with RMS less than 2.00 ms.

The limited infiltration at the LES suggests that there is a barrier to vertical soil moisture flow that impedes infiltration between 30 cm and 60 cm at the LES site. The lack of measured water content change at 60 cm and 90 cm is not equipment failure; both the 98n and 98 g probe profiles show little change in water content at 60 cm and 90 cm and it is unlikely that two pairs of probes at coincident depths are

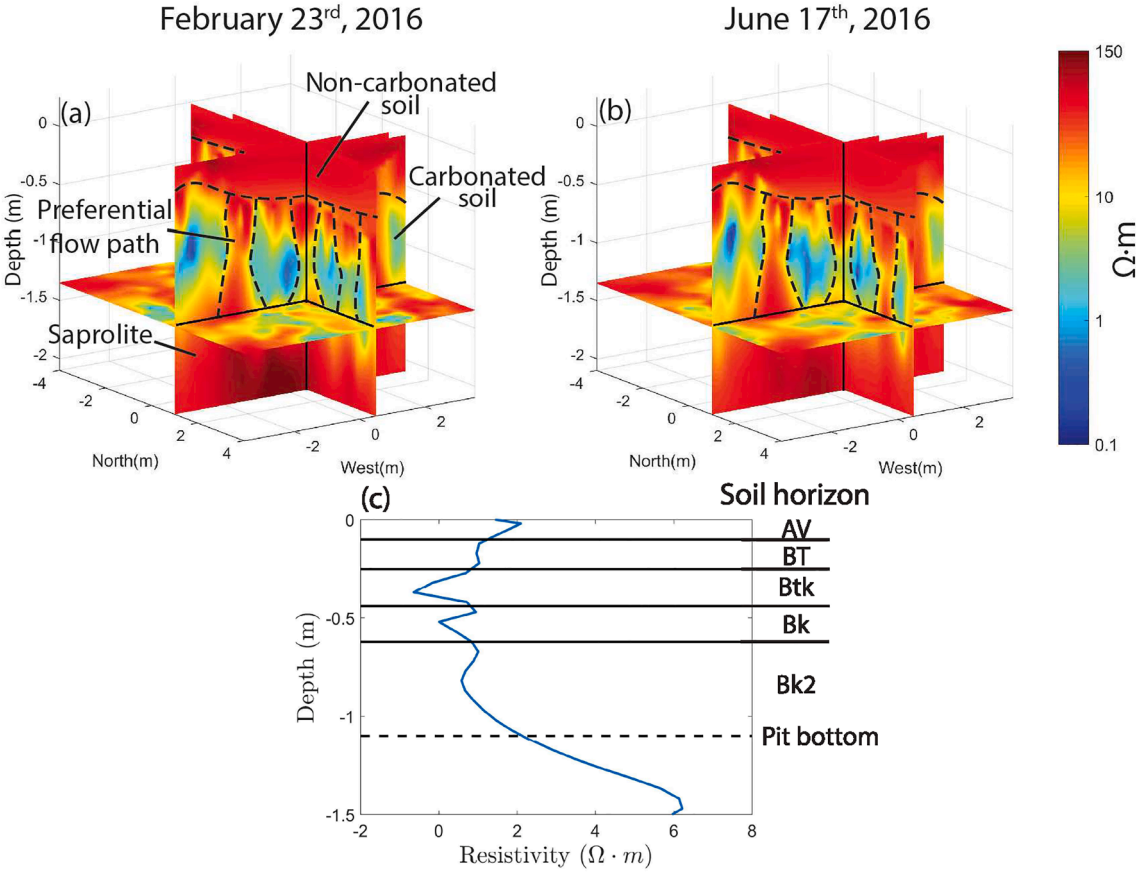

Fig. 4. The resistivity models from the static inversion of the February, 23rd, 2016 survey (a), June, 17th, 2016 survey (b), and (c) the 1D average difference of the (a) and (b) models at the LES site. The colorbar ramps are at a log scale but the values indicated on the colorbar are the true resistivity values, the color scales are the same for both (a) and (b). In (a) and (b) the dark dotted lines are the contact between the various soil structures and in (a) soil structures are labeled with our interpretation. The solid lines in (c) are at the depth of the soil horizons identified in the nearby soil pit. The soil moisture states are very different at the times these two surveys were taken, this is shown in both the measured soil moisture, see Fig. 2, and the difference in the vertical 1D average resistivity of the two models (c). While the soil moisture states are very different between the two surveys the resistivity structure remains largely the same. There are more preferential flow paths in the resistivity models than just the 3 highlighted in this figure. The changes in resistivity shown in (c) also correlate with the soil horizons found in the adjacent soil pit.

malfunctioning. In addition, the temperature measurements made by the CIDR probes agree closely with the temperature measurements made by the nearby temperature sensors used for the resistivity temperature correction. The CIDR probes within and outside the cattle exclosure show a similar seasonal soil moisture pattern, in which only the CIDR probes 30 cm and above measure any significant seasonal change in water content (Fig. 2).

The most notable feature observed in the soil pit near the ERT array was the transition between a B horizon with accumulated carbonate and clay (Btk), and a B horizon with accumulated carbonate (Bk) at 44 cm depth (Table 1). The boundary between the Btk and Bk layers is demarcated by a sharp increase in carbonate development, from stage I+ to IV respectively (Gile et al., 1966; Machette 1985). This abrupt transition from a stage I+ carbonate horizon (with diffuse precipitation of $CaCO_3$ filaments) to a stage IV carbonate horizon with platy, indurated, and massive structure is consistent with the discontinuous duripan layer that has been observed within the Reynolds Creek watershed (Seyfried et al., 2001). The boundary between the Btk and Bk layer at 44 cm is likely the barrier to flow identified by the CIDR probes.

The 2D resistivity profiles of the LES site (Fig. 5) show a general pattern of a moderately resistive 2 m top layer and a highly resistive middle layer. This pattern is interpreted as the soil layers transitioning from either mostly loess or a mixture of loess and weathered volcanic parent material to a less weathered and more resistive weathered basalt layer. In Fig. 5, the contours represent the seismic velocity from the SRT survey. Since weathering always reduces P-wave velocity of the parent material (Parsekian et al., 2015), we can assume that lower velocity material is more heavily weathered. The resistivity and the seismic velocity contours have a similar trend, and several structures are present in both the resistivity and velocity profiles. The north and east portions of the profiles show a decrease in both resistivity and seismic velocity; notably, a sharp increase in the depth of the 1000 m/s velocity contour. This change indicates that the north and west portions of the profile are more deeply weathered. There is also a high resistivity object near the surface at about easting (UTM X) 523350 m that coincides with a warping of the velocity contours. The 700 m/s velocity contour coincides with a transition from moderate resistivity to high resistivity in most of the profile, which is interpreted as the contact between loess-dominated soil and basalt saprolite. While there has not been as much research relating the degree of basalt weathering to seismic velocity (as compared to granite weathering), Von Voigtlander (2016) found that the basalt derived soils at dry sites on the Kohala Peninsula of Hawaii were no faster than 1 km/s. This research supports the interpretation that the 700 m/s velocity contour is the transition from soils to saprolite.

We superimposed the 3D resistivity models onto the 2D resistivity profiles where they are coincident (Fig. 5). The 3D resistivity data is the small rectangle of lower resistivity on the 2D profiles. The 3D resistivity models generally have lower resistivities than the 2D profiles. This is because the 2D survey has a much larger electrode spacing than the 3D grids, so the near surface low resistivities zone is not being well sampled by the 2D survey. The bottom of the grid of the 3D array is near the soil-saprolite boundary, so the primary zone of investigation is above the saprolite (Fig. 5).

The resistivity structure within the 3D ERT array is characterized by a <50 cm thick high resistivity top layer, underlain by a ~1.5 m thick low resistivity middle layer, and followed by a high resistivity layer at about 2 m depth (Fig. 4). The non-carbonate soil layers (including the Av and Bt horizons) observed in the soil pit (table 1) correspond with the high resistivity top layer, while the middle low resistivity layer correspond with the Btk, Bk, and Bk-2 soils (Fig. 6, Table 1). Below these units is the bottom high resistivity layer (Fig. 4), which we interpret to be the same feature as the saprolite layer identified in the 2D ERT and SRT (Fig. 5).

The high resistivity vertical pipe structures in the soil layer persist throughout all the 3D surveys no matter what inversion weighting strategy was applied. They can be seen in both the low resistivity winter (Fig. 4a) and the high resistivity summer, (Fig. 4b). As can be seen in Fig. 7c, the pipe structures persist throughout the seasons and their resistivities respond to precipitation. Therefore, we interpret the pipe structures as being preferential flow paths. The preferential flow paths were not observed in the soil pit, however sagebrush roots were observed at the bottom of the pit and the pit was dug in such a way as to minimize the impact on the sagebrush. Therefore, if the preferential flow paths are related to the sagebrush they would have been missed during our excavation.

During period of high soil moisture, due to the lower resistivity reducing the depth of current flow, the ERT's sensitivity at depth decreases. This reduces the number of the individual dipole–dipole measurements that measure the deeper portions of the profile (>1.0 m). The end result is a lower degree of confidence in the deeper resistivities during high soil moisture periods. However, the results from the static inversions, which are not constrained by a reference model, resolve the transition from soil to saprolite at the same depth regardless of the time of year. This suggests that while the sensitivity likely decrease at depth during wet periods, we still sample this portion of the profile well enough to resolve the soil lithology.

Table 1
Tabulated field and laboratory results from the soil pit, whose location is shown on Fig. 1 as a blue circle. The most notable feature is the sharp boundary between the Btk and Bk horizons, in which the carbonate stage changes from I+ to IV. This boundary also coincides with contact between the non-carbonate and carbonate soils identified in the 3D ERT, Figs. 4 and 5.

Depth (cm)	Horizon	Carbonate development	Upper boundary	Structure	Gravel (%)	Texture	Clay Films			Water % (H2O wt./Dry wt.)	Notes
							Amount	Distinctness	Location		
0–10	Av			m	<10	SIL				6	Well developed vesicules at 2 cm
10–25	Bt		c	abk sbk	<10	CL	1	d	pf	19.46	
25–44	Btk	I+	g	abk sbk	<10	SCL	1	d	pf	23.77	
44–62	Bk	IV	c	pl	25					21.77	
62–110	Bk-2	III	g	pl, m	25	LS				(16.01–13.4)	clasts increase with depth

c = clear, 2–5 cm thick
g = gradual, 5–15 cm thick
m = massive
abk = angular blocky
sbk = sub angular blocky
pl = platy
1 = Few Occupies 5–25% of the total area of the kind of surface described.
d = distinct
pf = Clay films occur on ped faces

Av = Vesicular A horizon
Bt = B horizon with accumulated clay
Btk = B horizon with accumulated carbonate and clay
Bk = B horizon with accumulated carbonate
SIC = Silty Clay
Cl = Clay Loam
SCL = Sandy Clay Loam
LS = Loamy Sand

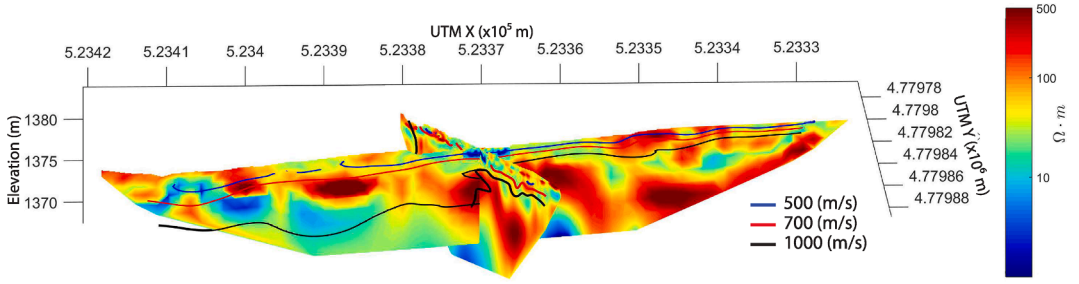

Fig. 5. Fence plot, looking north, of the 2D resistivity surveys with the seismic velocity contours from the SRT surveys overlain from the LES site surveys. The portion of the 2D resistivity proles that intersect the area of investigation of the 3D surveys, is replaced with the resistivites from the 3D resistivity models. The changes in seismic velocity and electrical resistivity are largely coincident.

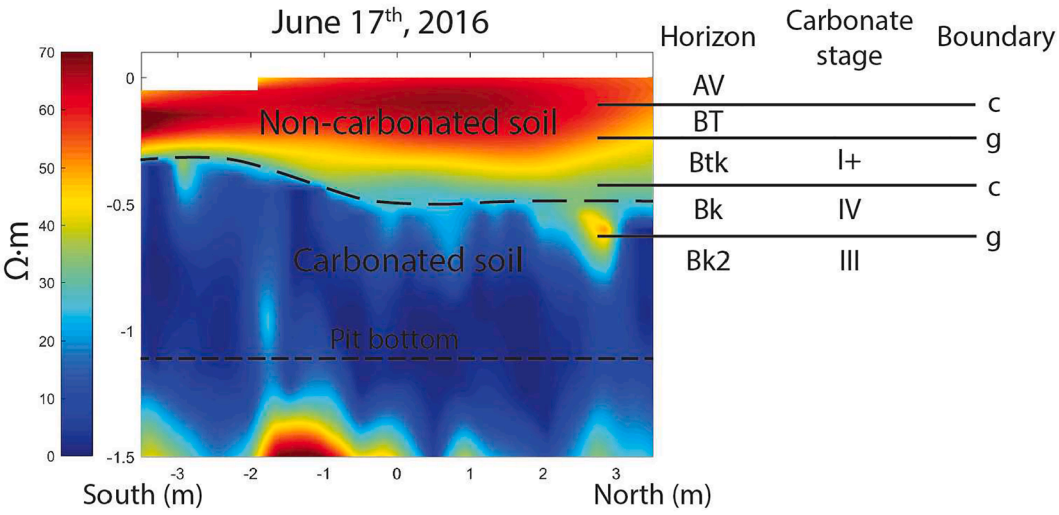

Fig. 6. North-south oriented slice of the middle of the static 3D ERT resistivity model gathered on June 17th, 2016, with the results from the soil pit plotted to the right. The boundary between the upper high resistivity layer, non-carbonated soil, and the low resistivity layer, carbonated soil, coincides with the boundary between the Btk and Bk soils overserved in the soil pit.

Preferential flow paths can be attributed to a variety of biological processes such as bioturbation, root channeling, and pedological processes like clay swelling and soil freezing that causes fractures to form in the soil (Jarvis, 2007). In addition, more extensive carbonate development and higher stages of carbonate accumulation (stage IV–stage V) is often characterized by brecciation and fracturing of the carbonate (e.g. Machette, 1985). Since the soils at this site below 10 cm rarely freeze, the preferential flow paths are unlikely to be caused by the freeze thaw cycle. Fracture networks from clay swelling do occur in highly clayey soils, like those observed at the LES site, however there is no reference in literature to suggest that these networks would form in vertical tube shape structures. There is no evidence of large burrows at this site and the pit was dug so that it would not disturb the sagebrush, so the soil pit did not show root-based bioturbation. Sagebrush roots, however, are the most likely candidate for the origins of the preferential flow paths. The vertical sagebrush roots, by growing through the consolidated carbonate soils could be providing a conductive pathway for moisture flow. The primary influence of roots on flow paths would not have been observed using traditional soil field methods such as soil pits or auguring, since these soil pits are typically placed to minimize vegetation disturbance.

The relationship between conductivity and water content is also different for the carbonate and non-carbonate soils. Fig. 8 shows the bulk conductivity vs volumetric water content measured at the CIDR probes near the ERT array from December 2008 to November 2017. The USDA Agricultural Research Service installed these probes in 2008 long before this experiment was conducted. What is apparent is that the relationship between bulk conductivity and volumetric water content for the soils at 5 cm and 15 cm is different from the relationship observed at 30 cm, 60 cm, and 90 cm. The slope of the relationship at 5 cm and 15 cm is 0.05 ($S/m/m^3/m^3$) and 0.07 ($S/m/m^3/m^3$), while at the deeper depths the slope is between 0.27 ($S/m/m^3/m^3$) and 0.36 ($S/m/m^3/m^3$). This suggests that the non-carbonate soils above 15 cm respond differently to soil moisture change than the carbonate soils below 30 cm. This suggests the two soils are chemically and/or structurally different; the geophysical results support the change in soil properties from the vesicular Av horizon to the clay and carbonate enhanced Btk horizon and the indurated Bk horizons. The ERT grids show that the preferential flow paths respond to soil moisture change in the same way as the non-carbonate soils (Figs. 7c and 9c).

5. Discussion

At most sites below the rain-snow transition at the RCCZO soil moisture profiles show that soil moisture infiltrates into the deeper subsurface. For example, at the Mid Elevation Sagebrush (MES) site, location shown in Fig. 1, the soil moisture can be seen to infiltrate through the depth of the profile, 90 cm, as shown in Fig. 3. At MES, and elsewhere within the RCCZO, we identify four characteristic soil moisture states: low, stable soil moisture, occasionally broken by rainstorms that infiltrate up to 15 cm; a late-fall or early-winter wetting period in which the field capacity of the soils is met and matrix flow propagates to the deeper soils; a wet, high-flux winter or early-spring period characterized by high matrix soil moisture and rapid soil moisture response to precipitation; a spring drying period in which precipitation decreases

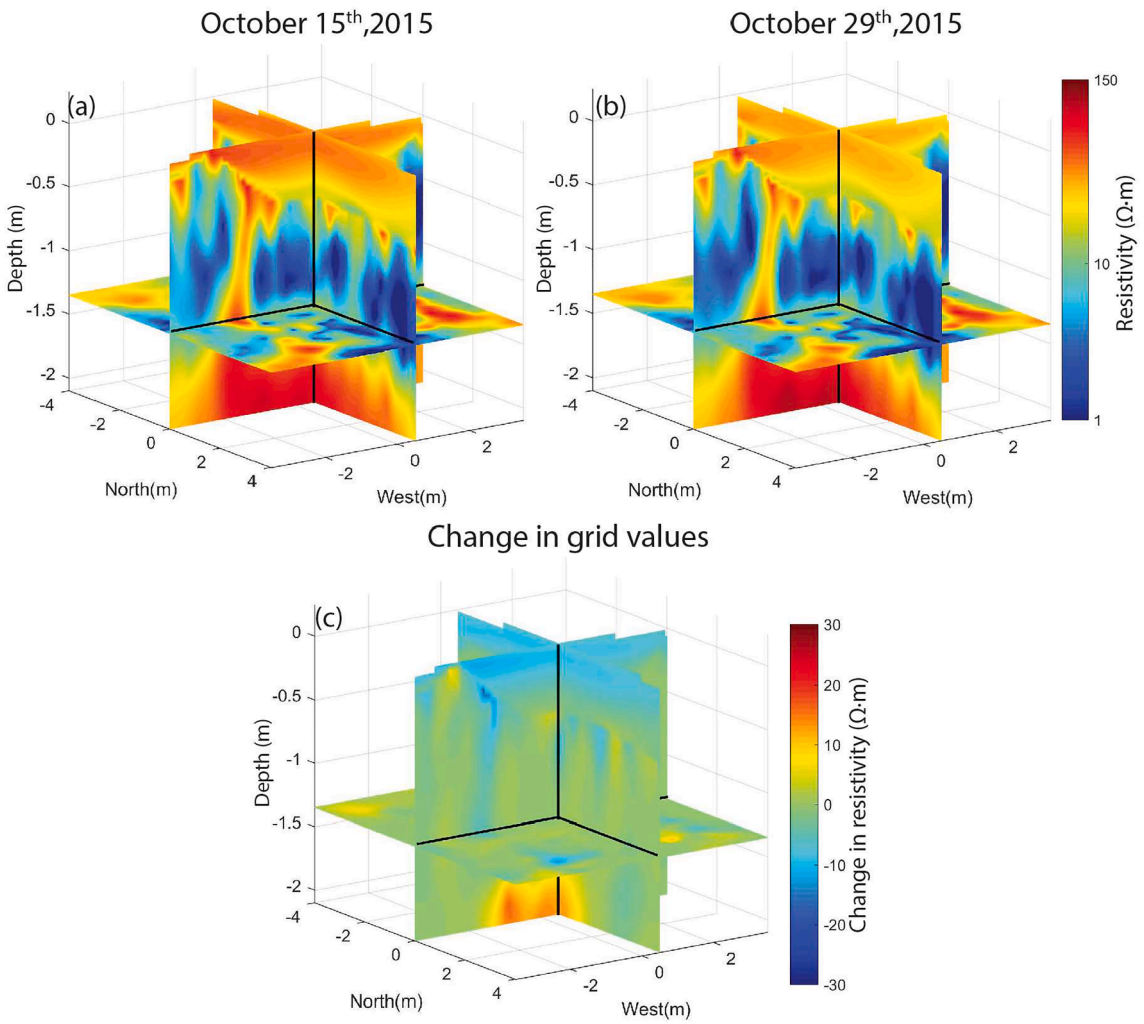

Fig. 7. The change in resistivity caused by the October 18th, 2015 rainfall event, which precipitated 10 mm rain at the LES site. The resistivity was measured before the rainfall on October 15th (a), and after the rainfall on October 29th (b). The change in resistivity between the two surveys is shown in panel (c). The changes in electrical resistivity is focused to the depositional layer and preferential flow paths. The resistivity color scales are the same for both (a) and (b).

and evapotranspiration draws down soil moisture to their summer dry values. There is little snow accumulation at both LES and MES, and the soils occasionally freeze, so there is no winter low flux period as was identified by McNamara et al., (2005). At the LES site, despite having similar precipitation types and amounts as the MES, there is no seasonal variation in soil moisture detected at the 60 cm and 90 cm deep soil moisture probes. This discrepancy suggests that something other than climactic factors are controlling the soil moisture infiltration at the LES site.

On October 18th, 2015, when the soils were dry and thought to be hydraulically disconnected a rainstorm precipitated 10 mm at the LES site. 3D ERT surveys were gathered before and after the rainstorm on October 15th and October 29th, see Fig. 7. Between those dates the CIDR probes show an increase in volumetric water content of about 20% at 5 cm, 15% at 15 cm, 5% at 30 cm and little change in water content at depths 60 cm and 90 cm. This change in water content is characteristic of a large rainstorm during the dry summer low flux period, in which meteoric water does not infiltrate into the deeper soils. The change in resistivity (Fig. 7c) follows a similar pattern: the highest change in resistivity is near the surface and decreases with depth extending to the bottom of the Bt horizon (soil characterized by some translocated clays but no significant calcium carbonate accumulations) at ~50 cm of depth. At ~50 cm depth, accumulation of pedogenic calcium carbonate in the soil creates a visible and measurable change in soil texture; and the Stage III carbonate accumulation (Gile et al., 1966; Machette, 1985) plugs soil pores and precipitates in platy, hard duripan layers within the soil (Table 1). The preferential flow path structures can also be seen decreasing in resistivity to a depth of ~1.25 m. However, the CIDR probes only observed significant changes in the volumetric water content in the upper 30 cm. Indicating that the preferential flow paths are providing a conduit for fluid flow during the summer low flux period that is not measured by the CIDR probes. This is subsurface flow that is being missed by the existing *in situ* instruments. It is likely that the soils within the preferential flow paths are the non-carbonate soils observed in the upper 30 cm. We hypothesize that the sage-brush roots created a vertical void, which filled with silty soil from the Av horizon and decayed root material filled either during the rooting process or after the roots died and decayed.

The seasonal changes in resistivity during the springs of 2015 and 2016 and the fall of 2015 are shown in Fig. 9. The spring 2015 change in resistivity is the difference in the resistivity models from May 29th and June 23rd. The spring 2016 is the difference in the grids from February 23rd, 2016 and June 29th, 2016. Lastly, the fall 2015 difference in the grids between the October 15th, 2015 and February 23rd, 2016 surveys. In both the spring (Fig. 9(a, b)) and fall (Fig. 9c) transitions, the ERT measured changes in resistivity focused to non-carbonated soil layer, preferential flow paths, and saprolite structures, while the CIDR only measured changes in volumetric water content in the upper 30 cm. The

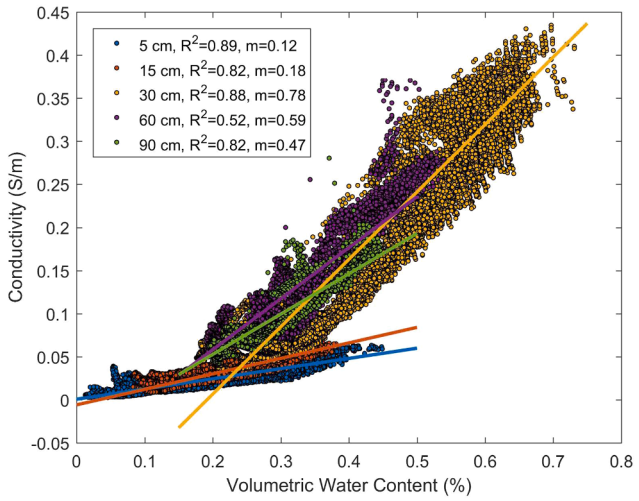

Fig. 8. The colored dots are the conductivity of the soils at varying water contents as measured by the CIDR probes, the color of the dot indicate the depth of the probes. Trend lines were fitted to the measurements at each depth and show that the soils can be grouped into two groups based on the slope of the conductivity vs. soil moisture trends. The conductivity of the shallow soils, 5 cm and 15 cm depth, responds less to changes in volumetric water content than the conductivity of the deeper soils and the deeper soils at 30 cm, 60 cm, and 90 cm.

lack of resistivity change in the carbonated soil layer indicates that they have a relatively constant volumetric water content. This constant electrical resistivity of the carbonated soils indicates again that the top of the carbonate soil is a barrier to moisture flow. If this soil structure was not the limiter in infiltration, then the seasonal changes in resistivity would decrease smoothly with depth reflecting a smooth soil moistures distribution.

The seasonal change in resistivity in the preferential flow paths also show that water is flowing through them. In addition, this change in water content is being missed by the CIDR probes. The corresponding decrease in resistivity of the preferential flow path and saprolite during the fall wetting (Fig. 9c), indicates that some amount of water is flowing through the preferential flow paths and wetting the saprolite. However, we cannot exclude the possibility that a mechanism other than preferential flow paths that is outside our survey area is the primary source of water traveling to the saprolite. During the spring 2016 drying period (Fig. 9b), the saprolite is decreasing in resistivity, suggesting that the saprolite is subject to evapotranspiration or that the moisture is infiltrating deeper and beyond the depth of investigation of our survey. This is not observed during the spring 2015 drying, but only the end of that season was surveyed with the 3D ERT. The seasonal changes in saprolite resistivity suggest that the deeper saprolites are hydraulically connected to the surface and shallow soils. If one were to only rely on the CIDR probes for interpretation, the logical conclusion would be that there is little to no infiltration to the deeper subsurface. Even so, the CIDR probes are not buried deep enough to measure the water content change in the saprolites, and as previously stated these probes are missing the flow through the preferential flow paths. The ERT shows that the preferential flow paths are providing a flow pathway in which some moisture is flowing through causing the saprolite to change in resistivity. The implications of the seasonal and precipitation driven changes in the resistivity models are that: (1) soil structure is a control on hydraulic connectivity, (2) that preferential flow paths are a hydraulic connection between the deep and shallow CZ that can be missed by *in situ* instruments, and (3) preferential flow paths flow can be initiated during the summer dry low flux period causing deep recharge. The observation that soil structure affects hydraulic connectivity and that preferential flow paths play a role in soil hydrology clearly plays an important role in the hydrology of this site. Within the Reynolds Creek watershed the total soil inorganic carbon is known to be variable at the pedon scale (Stanbery et al., 2017), so how carbonate soils affect soil hydrology could vary even within the LES site.

An additional caveat is that we are inferring soil moisture infiltration from changes in soil moisture and not measuring fluxes directly. And while the changes soil moisture are most likely caused by infiltration from the surface it is important to acknowledge that we are inferring this relationship.

Without using ERT the spatial complexities of the soil moisture dynamics could not have been observed, as *in site* measurement of water content can only provide data of a single point. Further *in site* instruments must be placed in direct contact with the soil they are measuring, this requires disrupting the soils either via digging or boring. This disruption can interfere with the soil moisture dynamics of the site. While installing the ERT arrays, electrodes disturbed the site's vegetation, 3 months after the array was installed the vegetation had recovered. Thus, the use of long term permanent ERT arrays allows for the non-invasive observation of soil hydrology over seasons. However, as with any geophysical study, proper interpretation of the ERT data required that we have the highly precise measurements provided by *in situ* instruments and the insight provided by direct observation of the soil.

6. Conclusion

McNamara et al. (2005) proposed five periods to describe the seasonal soil moisture characteristics. The seasonal periods at the LES site follow a similar pattern; however, the LES site does not accumulate snow so there is not a wet, low-flux period. Instead the pattern consists of: a dry summer and early-fall period, characterized by low stable soil moistures occasionally broken by rainstorms that infiltrate 15 cm; a late-fall or early-winter wetting period in which the field capacity of the soils is met and matrix flow propagates to the deeper soils; a wet high-flux winter early-spring, characterized by high matrix soil moistures and rapid soil moisture response to precipitation; and a spring drying period in which precipitation decreases and evapotranspiration draws soil moisture down to their summer dry values.

Using electrical resistivity surveys, we characterized the 3D soil moisture changes for all of the seasonal soil moisture periods, except for the late-fall/early-winter wetting period. However, the s late-fall/early-winter transition soil moisture changes are inferred from the surveys gathered before and after the transition. The soil moisture change in response to a substantial rainstorm during the dry summer state was also captured. These surveys captured the changing soil moisture structure at these sites in very high temporal and spatial density allowing us to better understand the soil structure soil moisture dynamic at the LES site.

The resistivity surveys show that at LES the seasonal and precipitation driven changes in resistivity are greatest within the persistent preferential flow paths that run through the carbonate soil and the upper layer of non-carbonate present at the site. Outside of the vertical preferential flow path structure, the resistivity of the carbonate soil layer does not change significantly, seasonally or otherwise. The CIDR probes show a similar pattern with depth, the probes at 5 cm, 15 cm and 30 cm measure changes in the volumetric water content, while the probes at 60 cm and 90 cm measure little change. This suggests that the top of the carbonate soil is a barrier to flow; hence, why the CIDR probes at 60 cm and 90 cm do not measure significant soil moisture change.

The resistivity of preferential flow paths can be seen to respond to single rainfall events and seasonal changes, suggesting that they provide a conduit of soil moisture flow. During the October 18th, 2015 precipitation event, the preferential flow paths can be seen to decrease in resistivity at depths up to 1.25 m, while the CIDR probes at the site do not show a change in soil moisture at 60 cm and 90 cm. This indicates that the preferential flow paths are allowing moisture to infiltrate into the deeper soils while bypassing the CIDR probes. The preferential flow

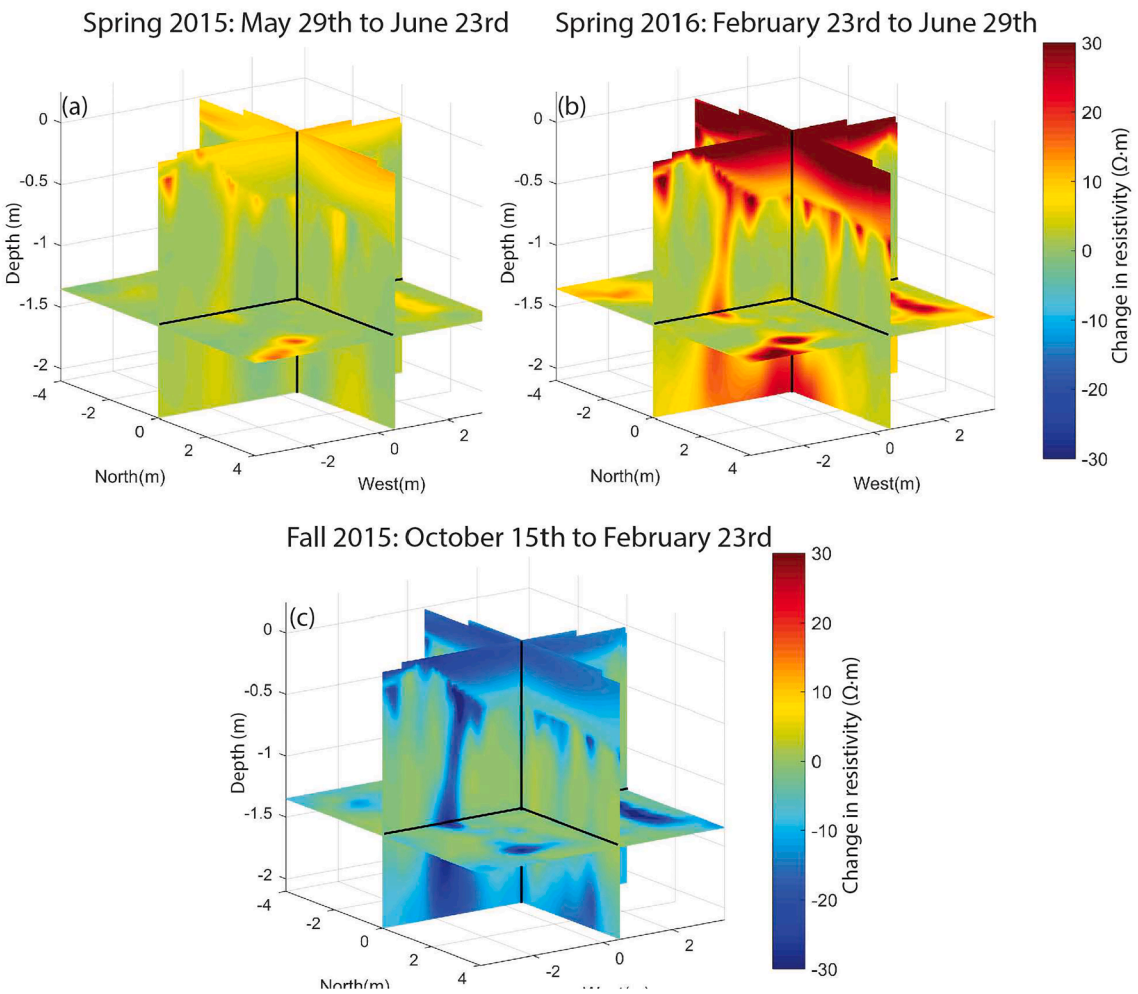

Fig. 9. The change in resistivity for the springs of 2015 and 2016 are shown in panels (a) and (b). The change for the spring of 2015 is the difference in the models from May 29th, 2015 to June 12th, 2015, and the change for the spring of 2016 is the difference between the models gathered on February, 23rd, 2016 and June 29th, 2016. The change in the resistivity for the fall 2015 is shown in panel (c). The fall 2015 model is the difference in the reistivity models gathered on October 15th, 2015 and February 23rd, 2016. The seasonal changes in electrical resistivity are focused to the depositional and preferential flow paths, suggesting that soil structure effects moisture distribution. The resistivity color scales are the same for all of the models shown.

paths can also be seen to change in resistivity during the fall wetting and spring drying. During the spring drying of 2015 and 2016, and the fall wetting, the CIDR measurements at 60 cm and 90 cm show minimal change in volumetric water content, while the preferential flow paths in the resistivity models show significant changes in resistivity at these depths. This indicates that the volumetric water content in the preferential flow paths is changing in response to seasonal soil moisture changes. Suggesting that preferential flow paths may allow for vertical soil moisture infiltration into the deeper soil profile during the fall wetting period, which is not captured by the CIDR measurements.

The time-lapse resistivity surveys show that at the LES site soil structure and soil weathering play a role in the flow and distribution of soil moisture, at both the seasonal and precipitation event timescales. A heavily carbonate soil is a barrier for moisture infiltration, and the preferential flow paths are seen to respond to precipitation and seasonal changes. It was previously observed with the CIDR probes that there was limited moisture infiltration into the deeper vadose zone, without the high spatial and temporal density time-lapse electrical resistivity gathered for this study it would have been difficult if not impossible to see the role that preferential flow paths and carbonate soils play in the soil moisture dynamics of this site. Given that high carbonate soils are relatively common throughout the western US and that time-lapse electrical resistivity are relatively uncommon, there is a potential that soil structure play an important and unknown role in the vadose zone hydrology in the western US.

Declaration of Competing Interest

The authors declare that they have no known competing financial interests or personal relationships that could have appeared to influence the work reported in this paper.

Acknowledgements

This study was conducted in collaboration and cooperation with the USDA Agriculture Research Service, Northwest Watershed Research Center, Boise, Idaho, and landowners within the Reynolds Creek Critical Zone Observatory (RCCZO). Support for this research was provided by the NSF via RC CZO Cooperative agreement NSF EAR-1331872. We would like to acknowledge Steve Van Vactor at the USDA ARS for providing the hydrologic data that made this work come together. As well as, Aida Mendieta, Paden Gould, Diego Domenzian, Hank Hetrick, Thomo Otheim, Johnathan Dick, Emily Romero, and Ryan Will for their help in the field.

References

al Hagrey, S.A., Michaelsen, J., 1999. Resistivity and percolation study of preferential flow in vadose zone at Bokhorst, Germany. Geophysics 64 (3), 746–753.

al Hagrey, S.A., Schubert-Klempnauer, T., Wachsmuth, D., Michaelsen, J., Meissner, R., 1999. Preferential flow: First results of a full-scale flow model. Geophys. J. Int. 138 (3), 643–654.

Amidu, S.A., Dunbar, J.A., 2007. Geoelectric studies of seasonal wetting and drying of a Texas vertisol. Vadose Zone J. 6 (3), 511–523. https://doi.org/10.2136/vzj2007.0005.

Brillante, L., Bois, B., Mathieu, O., Bichet, V., Michot, D., Lévêque, J., 2014. Monitoring soil volume wetness in heterogeneous soils by electrical resistivity. A field-based pedotransfer function. J. Hydrol. 516, 56–66. https://doi.org/10.1016/j.jhydrol.2014.01.052.

Brunet, P., Clément, R., Bouvier, C., 2010. Monitoring soil water content and deficit using Electrical Resistivity Tomography (ERT) – A case study in the Cevennes area, France. J. Hydrol. 380 (1–2), 146–153. https://doi.org/10.1016/j.jhydrol.2009.10.032.

Calamita, G., Brocca, L., Perrone, A., Piscitelli, S., Lapenna, V., Melone, F., Moramarco, T., 2012. Electrical resistivity and TDR methods for soil moisture estimation in central Italy test-sites. J. Hydrol. 454–455, 101–112. https://doi.org/10.1016/j.jhydrol.2012.06.001.

Cassiani, G., Deiana, R., Villa, A., Bruno, V., Bagliani, A., Miorali, M., and Fusi, N. (2006). A water injection experiment in the vadose zone: The use and value of non invasive cross-hole data for model calibration. In Proc. Int. Conf. on Computational Methods in Water Resour., 16th, Copenhagen, Denmark (pp. 19–22). Retrieved from http://proceedings.dtu.dk/fedora/repository/dtu:1634/OBJ/article.pdf.

Daily, W., Ramirez, A., LaBrecque, D., Nitao, J., 1992. Electrical resistivity tomography of vadose zone water movement. Water Resour. Res. 28 (5), 1429–1442.

Deiana, R., Cassiani, G., Kemna, A., Villa, A., Bruno, V., Bagliani, A., 2007. An experiment of non-invasive characterization of the vadose zone via water injection and cross-hole time-lapse geophysical monitoring. Near Surf. Geophys. 5 (3), 183–194.

Dietrich, W.E., Bellugi, D.G., Sklar, L.S., Stock, J.D., Heimsath, A.M., Roering, J.J., 2003. Geomorphic transport laws for predicting landscape form and dynamics. In: Wilcock, P.R., Iverson, R.M. (Eds.), Geophysical Monograph Series, Vol. 135. American Geophysical Union, Washington, D. C., pp. 103–132. http://www.agu.org/books/gm/v135/135GM09/135GM09.shtml

Fan, J., Scheuermann, A., Guyot, A., Baumgartl, T., Lockington, D.A., 2015. Quantifying spatiotemporal dynamics of root-zone soil water in a mixed forest on subtropical coastal sand dune using surface ERT and spatial TDR. J. Hydrol. 523, 475–488. https://doi.org/10.1016/j.jhydrol.2015.01.064.

Freer, J., McDonnell, J.J., Beven, K.J., Peters, N.E., Burns, D.A., Hooper, R.P., Aulenbach, B., Kendall, C., 2002. The role of bedrock topography on subsurface storm flow: The role of bedrock topography on subsurface storm flow. Water Resour. Res. 38 (12), 5-1–5-16. https://doi.org/10.1029/2001WR000872.

French, H., Binley, A., 2004. Snowmelt infiltration: monitoring temporal and spatial variability using time-lapse electrical resistivity. J. Hydrol. 297 (1–4), 174–186. https://doi.org/10.1016/j.jhydrol.2004.04.005.

Gile, L.H., Peterson, F.F., Grossman, R.B., 1966. Morphological and genetic sequences of carbonate accumulation in desert soils. Soil Sci. 101 (5), 347–360.

Hansen, B.P., Lane, J.W., 1995. Use of surface and borehole geophysical surveys to determine fracture orientation and other site characteristics in crystalline bedrock terrain, Millville and Uxbridge. US Department of the Interior, US Geological Survey, Massachusetts. https://pubs.usgs.gov/wri/1995/4121/report.pdf.

Hinckley, E.-L., Ebel, B.A., Barnes, R.T., Anderson, R.S., Williams, M.W., Anderson, S.P., 2014. Aspect control of water movement on hillslopes near the rain-snow transition of the Colorado Front Range: Snowmelt and hydrological flow paths on opposing hillslope aspects. Hydrol. Process. 28 (1), 74–85. https://doi.org/10.1002/hyp.v28.110.1002/hyp.9549.

Holbrook, W.S., Riebe, C.S., Elwaseif, M., L. Hayes, J., Basler-Reeder, K., L. Harry, D., Malazian, A., Dosseto, A., C. Hartsough, P., W. Hopmans, J., 2014. Geophysical constraints on deep weathering and water storage potential in the Southern Sierra Critical Zone Observatory: Geophysical constraints on weathering in the Southern Sierra CZO. Earth Surf. Proc. Land. 39 (3), 366–380. https://doi.org/10.1002/esp.3502.

Jarvis, N.J., 2007. A review of non-equilibrium water flow and solute transport in soil macropores: principles, controlling factors and consequences for water quality. Eur. J. Soil Sci. 58 (3), 523–546. https://doi.org/10.1111/ejs.2007.58.issue-310.1111/j.1365-2389.2007.00915.x.

Johnson, T.C., Versteeg, R.J., Ward, A., Day-Lewis, F.D., Revil, A., 2010. Improved hydrogeophysical characterization and monitoring through parallel modeling and inversion of time-domain resistivity andinduced-polarization data. Geophysics 75 (4), WA27–WA41. https://doi.org/10.1190/1.3475513.

Kean, W.F., Waller, M.J., Layson, H.R., 1987. Monitoring moisture migration in the vadose zone with resistivity. Groundwater 25 (5), 562–571.

Keller, G.V., Frishchknecht, F.C., 1966. Electrical methods in geophysical prospecting. Pergamon Press, Oxford.

Leslie, I.N., Heinse, R., 2013. Characterizing soil–pipe networks with pseudo-three-dimensional resistivity tomography on forested hillslopes with restrictive horizons. Vadose Zone J. 12 (4) https://doi.org/10.2136/vzj2012.0200.

Machette, M., 1985. Calcic soils of southwestern United States. Special Pap. Geol. Society of America 203, 1–21.

McIntyre, D.H., 1972. Cenozoic geology of the Reynolds Creek Experimental Watershed, Owyhee County, Idaho. Idaho Buraeu of Mines and Geology, Pamphlet, p. 151.

McNamara, J.P., Chandler, D., Seyfried, M., Achet, S., 2005. Soil moisture states, lateral flow, and streamflow generation in a semi-arid, snowmelt-driven catchment. Hydrol. Process. 19 (20), 4023–4038. https://doi.org/10.1002/(ISSN)1099-108510.1002/hyp.v19:2010.1002/hyp.5869.

Michot, D., Benderitter, Y., Dorigny, A., Nicoullaud, B., King, D., Tabbagh, A., 2003. Spatial and temporal monitoring of soil water content with an irrigated corn crop cover using surface electrical resistivity tomography: Soil water study using electrical resistivity. n/a-n/a Water Resour. Res. 39 (5). https://doi.org/10.1029/2002WR001581.

Miller, C.R., Routh, P.S., Brosten, T.R., McNamara, J.P., 2008. Application of time-lapse ERT imaging to watershed characterization. Geophysics 73 (3), G7–G17. https://doi.org/10.1190/1.2907156.

Monego, M., Cassiani, G., Deiana, R., Putti, M., Passadore, G., Altissimo, L., 2010. A tracer test in a shallow heterogeneous aquifer monitored via time-lapse surface electrical resistivity tomography. Geophysics 75 (4), WA61–WA73. https://doi.org/10.1190/1.3474601.

Niemeyer, R.J., Heinse, R., Link, T.E., Seyfried, M.S., Klos, P.Z., Williams, C.J., Nielson, T., 2017. Spatiotemporal soil and saprolite moisture dynamics across a semi-arid woody plant gradient. J. Hydrol. 544, 21–35. https://doi.org/10.1016/j.jhydrol.2016.11.005.

Nijland, W., van der Meijde, M., Addink, E.A., de Jong, S.M., 2010. Detection of soil moisture and vegetation water abstraction in a Mediterranean natural area using electrical resistivity tomography. CATENA 81 (3), 209–216. https://doi.org/10.1016/j.catena.2010.03.005.

Olona, J., Pulgar, J.A., Fernández-Viejo, G., López-Fernández, C., González-Cortina, J.M., 2010. Weathering variations in a granitic massif and related geotechnical properties through seismic and electrical resistivity methods. Near Surf. Geophys. 8 (6), 585–599. https://doi.org/10.3997/1873-0604.2010043.

Parsekian, A.D., Singha, K., Minsley, B.J., Holbrook, W.S., Slater, L., 2015. Multiscale geophysical imaging of the critical zone: Geophysical imaging of the critical zone. Rev. Geophys. 53 (1), 1–26. https://doi.org/10.1002/2014RG000465.

Robinson, D.A., Campbell, C.S., Hopmans, J.W., Hornbuckle, B.K., Jones, S.B., Knight, R., Ogden, F., Selker, J., Wendroth, O., 2008. Soil moisture measurement for ecological and hydrological watershed-scale observatories: A review. Vadose Zone J. 7 (1), 358–389. https://doi.org/10.2136/vzj2007.0143.

Robinson, J., Johnson, T., Slater, L., 2013. Evaluation of known-boundary and resistivity constraints for improving cross-borehole DC electrical resistivity imaging of discrete fractures. Geophysics 78 (3), D115–D127. https://doi.org/10.1190/geo2012-0333.1.

Robinson, J.L., Slater, L.D., Schäfer, K.V.R., 2012. Evidence for spatial variability in hydraulic redistribution within an oak–pine forest from resistivity imaging. J. Hydrol. 430–431, 69–79. https://doi.org/10.1016/j.jhydrol.2012.02.002.

Sasaki, Y., 1992. Resolution of resistivity tomography inferred from numerical simulation. Geophys. Prospect. (Eur. Assoc. Explorat. Geophys.) 40 (4), 453.

Schuster, G., Quintus-Bosz, A., 1993. Wavepath eikonal traveltime inversion: Theory. Geophysics 58 (9), 1314–1323.

Schwartz, B.F., Schreiber, M.E., Yan, T., 2008. Quantifying field-scale soil moisture using electrical resistivity imaging. J. Hydrol. 362 (3–4), 234–246. https://doi.org/10.1016/j.jhydrol.2008.08.027.

Seyfried, M.S., Hanson, C.L., Murdock, M.D., Van Vactor, S., 2001. Long-Term Lysimeter Database, Reynolds Creek Experimental Watershed, Idaho, United States.pdf. Water Resour. Res. 37 (11), 2853–2856.

Sidle, R.C., Noguchi, S., Tsuboyama, Y., Laursen, K., 2001. A conceptual model of preferential flow systems in forested hillslopes: evidence of self-organization. Hydrol. Process. 15 (10), 1675–1692. https://doi.org/10.1002/hyp.233.

Singha, K., Gorelick, S.M., 2005. Saline tracer visualized with three-dimensional electrical resistivity tomography: Field-scale spatial moment analysis: Spatial moment analysis of ERT. n/a-n/a Water Resour. Res. 41 (5). https://doi.org/10.1029/2004WR003460.

Srayeddin, I., Doussan, C., 2009. Estimation of the spatial variability of root water uptake of maize and sorghum at the field scale by electrical resistivity tomography. Plant Soil 319 (1–2), 185–207. https://doi.org/10.1007/s11104-008-9860-5.

Stanbery, Christopher Allen, 2016. Controls on the Presence, Concentration, Storage, and Variability of Soil Inorganic Carbon in a Semi-Arid Watershed. Boise State University Theses and Dissertations. 1233.

Stanbery, C.A., Pierce, J.L., Benner, S.G., Lohse, K., 2017. On the rocks: Quantifying storage of inorganic soil carbon on gravels and determining pedon-scale variability. CATENA 157, 436–442. https://doi.org/10.1016/j.catena.2017.06.011.

Travelletti, J., Sailhac, P., Malet, J.-P., Grandjean, G., Ponton, J., 2012. Hydrological response of weathered clay-shale slopes: water infiltration monitoring with time-lapse electrical resistivity tomography. Hydrol. Process. 26 (14), 2106–2119. https://doi.org/10.1002/hyp.7983.

Tromp-van Meerveld, H.J., McDonnell, J.J., 2006a. Threshold relations in subsurface stormflow: 1. A 147-storm analysis of the Panola hillslope: Subsurface flow relations, 1. Water Resour. Res. 42 (2), n/a-n/a. https://doi.org/10.1029/2004WR003778.

Tromp-van Meerveld, H.J., McDonnell, J.J., 2006b. Threshold relations in subsurface stormflow: 2. The fill and spill hypothesis. Water Resour. Res. 42 (2), n/a-n/a. https://doi.org/10.1029/2004WR003800.

Uhlemann, S., Chambers, J., Wilkinson, P., Maurer, H., Merritt, A., Meldrum, P., Kuras, O., Gunn, D., Smith, A., Dijkstra, T., 2017. Four-dimensional imaging of moisture dynamics during landslide reactivation: Imaging of Landslide Moisture Dynamics. J. Geophys. Res. Earth Surf. 122 (1), 398–418. https://doi.org/10.1002/2016JF003983.

Von Voigtlander, J., 2016. P-wave velocity of weathering profiles from a basalt climosequence: Implications for weathering on the mechanical properties of the

critical zone. Retrieved from https://deepblue.lib.umich.edu/handle/2027.42/116847.

Yamakawa, Y., Kosugi, K., Katsura, S., Masaoka, N., Mizuyama, T., 2012. Spatial and Temporal Monitoring of Water Content in Weathered Granitic Bedrock Using Electrical Resistivity Imaging. Vadose Zone J. 11 (1) https://doi.org/10.2136/vzj2011.0029.

Zumr, D., Snehota, M., Cislerova, M., 2012. Numerical simulation of tension infiltration experiment monitored by 3D ERT. Presented at the 5th Asia-Pacific Conference on Unsaturated Soils. Retrieved from https://www.researchgate.net/profile/David_Zumr/publication/271194536_Numerical_simulation_of_tension_infiltration_experiment_monitored_by_3D_ERT/links/54bfc6e10cf28eae4a661a87.pdf.